AFRL-MN-EG-TR-2004-7025

SiC MEMS for Harsh Environments

Kenneth C. Bradley
Scott L. Roberson
Donald R. Wiff

AFRL/MNMF
Eglin AFB, FL 32542-6810
AFRL/MLPS
Wright-Patterson AFB, OH 45433-7707

DECEMBER 2003

FINAL REPORT FOR PERIOD MARCH 2000 – DECEMBER 2003

AIR FORCE RESEARCH LABORATORY, MUNITIONS DIRECTORATE

Air Force Materiel Command ■ United States Air Force ■ Eglin Air Force Base

Report Documentation Page

Form Approved
OMB No. 0704-0188

1. REPORT DATE	2. REPORT TYPE	3. DATES COVERED
DEC 2003		**-**

4. TITLE AND SUBTITLE	5a. CONTRACT NUMBER
SiC MEMS FOR HARSH ENVIRONMENTS	5b. GRANT NUMBER
	5c. PROGRAM ELEMENT NUMBER **61102F**

6. AUTHOR(S)	5d. PROJECT NUMBER
KENNETH BRADLEY; SCOTT ROBERSON; DONALD WIFF	**2305**
	5e. TASK NUMBER **PM**
	5f. WORK UNIT NUMBER **01**

7. PERFORMING ORGANIZATION NAME(S) AND ADDRESS(ES)	8. PERFORMING ORGANIZATION REPORT NUMBER
AIR FORCE RESEARCH LABORATORY,AFRL/MNMF at Eglin AFB, FL & AFRL/MLPS at Wright-Patterson AFB, OH 45433-7707,306 W. EGLIN BLVD.,EGLIN AFB,FL,32542-5430	**SAME AS BLOCK 11**

9. SPONSORING/MONITORING AGENCY NAME(S) AND ADDRESS(ES)	10. SPONSOR/MONITOR'S ACRONYM(S)
	11. SPONSOR/MONITOR'S REPORT NUMBER(S)

12. DISTRIBUTION/AVAILABILITY STATEMENT

Approved for public release; distribution unlimited

13. SUPPLEMENTARY NOTES

14. ABSTRACT

This document is the final technical report for the SiC MEMS for Harsh Environments in-house research program jointly coordinated between AFRL/MNMF and AFRL/MLPS, and addresses the benefits of silicon carbide (SiC) as a material of choice for harsh environment applications, specifically at the scale of microelectromechanical systems (MEMS). The results from this program provide clear evidence of the benefit of SiC as a harsh environment (specifically high temperature) material for both structural and electronic devices. Although shock testing of SiC MEMS devices under this program was not accomplished, subsequent work allowed for this testing to occur, with positive results. Furthermore, one of the key concerns with respect to SiC electronics was the need for good contact metallization for ohmic contacts. Rhenium was found to be an excellent material for providing ohmic contact metallization on SiC. These results provide a good foundation for the benefits of SiC for harsh environment (high temperature and high shock) applications

15. SUBJECT TERMS

16. SECURITY CLASSIFICATION OF:			17. LIMITATION OF ABSTRACT	18. NUMBER OF PAGES	19a. NAME OF RESPONSIBLE PERSON
a. REPORT	b. ABSTRACT	c. THIS PAGE			
unclassified	**unclassified**	**unclassified**		**26**	

NOTICE

When Government drawings, specifications, or other data are used for any purpose other than in connection with a definitely Government-related procurement, the United States Government incurs no responsibility or any obligation whatsoever. The fact that the Government may have formulated or in any way supplied the said drawings, specifications, or other data, is not to be regarded by implication, or otherwise in any manner construed, as licensing the holder, or any other person or corporation; or as conveying any rights or permission to manufacture, use, or sell any patented invention that may in any way be related thereto.

This technical report is releasable to the National Technical Information Services (NTIS). At NTIS it will be available to the general public, including foreign nations.

This technical report has been reviewed and is approved for publication.

FOR THE COMMANDER

//Signed//	//Signed//	//Signed//
Mr. Paul K. Laird	Mr. Timothy M. Tobik	Lt Kenneth C. Bradley
Technical Director	Technical Advisor	Program Manager
Ordnance Division	Fuzes Branch	Fuzes Branch

Anyone having need for a copy of this report should first contact the Defense Technical Information Center (DTIC) at the address shown below. If you are a registered DTIC User, DTIC can provide you with a copy. Please do not request copies from the Air Force Research Laboratory, Munitions Directorate. Requests for additional copies should be directed to:

Defense Technical Information Center (DTIC)
8725 John J. Kingman Road, Ste 0944
Ft Belvoir, VA 22060-6218

This report is published in the interest of the scientific and technical information exchange. Publication of this report does not constitute approval or disapproval of the ideas or findings

NOTE TO AGENCIES ON DISTRIBUTION LIST: If your address has changed, if you wish to be removed from our mailing list, or if your organization no longer employs the addressee, please notify AFRL/MNMF, 101 W. Eglin Blvd., Eglin AFB FL 32542-6810, to help us maintain a current mailing list.

a. REPORT	b. ABSTRACT	c. THIS PAGE			19b. TELEPHONE NUMBER *(include area code)*
UNCLASSIFED	UNCLASSIFIED	UNCLASSIFIED	SAR	26	850-883-0039 (DSN 873-0039)

Standard Form 298 (Rev. 8-98)
Prescribed by ANSI Std. Z39.18

Table of Contents

List of Figures

1 INTRODUCTION

1.1 Overview

This document is the final technical report for the SiC MEMS for Harsh Environments in-house research program jointly coordinated between AFRL/MNMF and AFRL/MLPS.

This document addresses the benefits of silicon carbide (SiC) as a material of choice for harsh environment applications, specifically at the scale of microelectromechanical systems (MEMS). Although all of the objectives of this research were not fully met, due to fabrication issues associated with this relatively new technology, the main objective of establishing the benefit of SiC for harsh environment applications was a successful accomplishment of this program.

1.2 Objective

The objective of this 6.1 effort was to investigate the survivability limits of SiC MEMS and electronics for harsh environments, in order to gain a fundamental understanding of the failure modes and temperature limits for SiC structural and electronic components. Devices were to be fabricated and evaluated under high g loads to determine failure mechanisms and operation limits.

1.3 Accomplishments

Due to unforeseeable fabrication issues associated with the SiC MEMS foundry, the desired devices were not fabricated. Consequently, high g shock loading of the SiC MEMS devices was not accomplished. However, high temperature material characterization was accomplished on two distinct polytypes of SiC (3C poly-SiC and 6H), and this was compared to similar characterization of polysilicon. The results of this characterization, as presented in this document, give clear evidence of the benefit of SiC for high temperature environments. A subsequent program has allowed for high g shock loading of a functioning SiC MEMS accelerometer, with published results [1].

2 HIGH TEMPERATURE TESTING OF SiC

Measuring Young's modulus of various SiC polymorphs over a wide temperature range (100 to 600 °C) has been accomplished using a Bohlin rheometer in the torsion mode. With Young's modulus as a function of temperature, and using software such as MemCad, by Coventor, Inc., one can simulate the resonance frequencies of a given MEMS microaccelerometer design. These frequencies are related to natural vibrations of the system and vary when a constant or sinusoidal force is applied to the system. Correlations of predicted resonances with experimental data from high impact are presented.

2.1 Introduction

In many industrial and military applications there is a need to have MEMS sensors that can withstand high shock, 80,000g's and temperatures close to 1000 °C. A material of choice is silicon carbide (SiC). As technology pushes toward space and harsh environment applications, the need for high power, high temperature, radiation resistant, and high mechanical performance materials has become a motivation in materials research for electronic and mechanical performance of nano/microelectromechanical systems. High thermal conductivity and excellent durability makes silicon carbide an excellent choice for these applications. Since SiC has a bandgap that is dependant upon its polytype, it is considered a versatile and competitive material [2-8] for applications where other conventional semiconductors fail. Its high electron mobility allows for increase current within the semiconductor and high energy pulsed applications [9]. Polytypes range from purely wurtzite (cubic) to hexagonal with over 200 variations [10]. The bandgap ranges from 2.3 to 3.3 eV depending on the polytype with the most common types being 3C-SiC (2.3 eV) and 6H-SiC (2.9 eV). SiC has a melting temperature of approximately 2800 °C, thus capable of being operated in the temperature range of 600-1000 °C [4,5].

The need for the mechanical properties (modulus) of these SiC polytypes at a series of temperatures (room temperature to 600 °C) led us to consider the torsion solid fixturing device found in rheometers such as a Bohlin Rheometer. Equipped with a high temperature oven, and operating at either a fixed frequency, this instrument yielded to he shear modulus, G', which for elastic materials and small rectangular cross-sections G' = 3E, where E is the elastic modulus, or Young's modulus. For low modulus materials such as rubber, the problem of twisting of a bar of rectangular cross section is complicated due to the warping of the cross section during twisting [11]. When there is longitudinal tension and the material is soft, there is still another correction needed [12]. However, for very rigid materials such as silicon or silicon carbide, these conditions do not cause significant deviations from the true modulus.

Once the modulus versus temperature for various SiC polytypes, silicon, and polysilicon were obtained, single values of modulus and the corresponding temperatures were used as input to Coventor, Inc.'s software for MEMS simulation, MemCad version 4.0. This software was used to simulate the performance of a capacitive microaccelerometer design fabricated from poly (3C-SiC) by Case-Western Reserve University [13] (see Fig. 1). The modulus and temperature were stored in the MemCad material property data files. Simulations to obtain natural frequencies, resonance frequencies while impinging a 1 MPa load on the upper parallel plate applying a 10V potential across the plates were then performed [14].

Once these resonance frequency results were obtained for silicon, polysilicon, 6H-SiC and poly (3C-SiC) at various temperatures and under different external forces, they were compared with our experimental impact test resulted in an effort to better understand the performance of microaccelerometers under real life applications.

2.2 Measurements and Computations

The Bohlin VOR-MELT rheometers used for mechanical modulus measurements had a solids fixture, which held both ends of a vertically oriented rectangular cross section bar (5.23x0.58x8.6 cm). The 8.6 cm was the length of the specimen between the top and bottom clamps. The torque element was 51 g-cm, temperature ranged from 30 to 350 °C, at a 0.5 °C per minute heating rate, measurement interval was 60 sec, sensitivity was 1x, and the amplitude of oscillation was 10%. The measurements were made in the oscillation test mode. Typical results are shown in Fig. 2. The modulus, E, was determined by using the equation G' = 3E.

The software used in these simulations was MemCad v 4.0, by Microcosm Inc., now Coventor, Inc. A *.cif file of the CWRU capacitive microaccelerometer shown in Figure 1 was designed with L-Edit software by Tanner Associates. This was used as input to the MemCad process modeler or KIC layout editor. The results were transferred to the IDEAS solid modeler package in MemCad. This provided the solid model on which finite element modeling could be performed. Modal and harmonic analyses were performed on the unperturbed model and when a 1 MPa load or a 10 V potential were independently applied to the system. For a steady state linear dynamic analysis, the equation of motion for the αth mode is:

$$\ddot{x}_a + c_a \dot{x} + w_a^2 x = \frac{1}{m_a} f_a e^{i\Omega t}$$

where, x_a is the amplitude of the mode α, c_a is the damping coefficient associated with this mode, w_a is the undamped frequency of this mode, m_a is the generalized mass associated with the mode, f_a is the amplitude of forcing associated with the mode, and Ω is a forcing frequency. Steady state response is given as a frequency sweep through a user-specified range of frequencies.

2.3 Results of Computation

The natural frequency modes of polysilicon at room temperature (30 °C) and 200 °C are about the same (see Table 1). This is because the modulus of polysilicon at these two temperatures is nearly equal. However, poly (3C-SiC) has a much higher modulus than polysilicon and as a result, even at 300 °C, the resonance frequencies are higher than those of polysilicon.

During real life usage, there will be external forces on the device, so we imposed a 1 MPa force on the top plate to see what effect this would have on the resonance frequencies. As can be seen in Table 2, applying a 1 MPa force to the top plate reduces the resonance frequencies by a factor of 10^7. This was true in spite of the increased modulus of the poly (3C-SiC). As a rough

estimate, since force equals the product of mass and acceleration (g = 9.8 m/sec^2), a 1 MPa force corresponds to about 100,000g's. High speed impact testing has resulted decelerations of up to 80,000g's.

Finally, in Table 3 we show the reaction forces at the ends of the tethers, where the upper plate is fastened to the device frame (see Fig. 3). In all cases, the application of a 10 V potential across the parallel plate capacitor and the application of 1 MPa to the upper plate resulted in roughly the same in-plane forces (~0.4 μN) and a vertical force of 301 μN.

Table 1. Natural resonance frequencies for the capacitive microaccelerometer.

Semiconductor	Temperature	Frequency (Hz)				
	(C)	1	2	3	4	5
Poly silicon	30	5,310	9.590	9,670	29,300	42,400
	200	5,300	9,560	9,640	29,300	42,300
Poly(3C-SiC)	300	10,100	18,300	18,500	57,400	79,100

Table 2. Resonance frequencies for capacitive microaccelerometer with 1 MPa applied to the top plate.

Semiconductor	Temperature	Frequency (Hz)				
	(C)	1	2	3	4	5
Poly(3C-SiC)	500	0.00024	0.00037	0.00039	0.00053	0.00053
	1000	0.00017	0.00030	0.00030	0.00092	0.00133

Table 3. Reaction forces at end of tether when external forces are applied.

Semiconductor	Temperature	External	Forces (μN)		
	(C)	Force	F_x	F_y	F_z
Poly silicon	30	10 Volt	0.427	-0.493	301.41
Poly(3C-SiC)	500	1 MPa	0.349	-3.46	301.80
	1000	1 MPa	0.352	-3.45	301.79

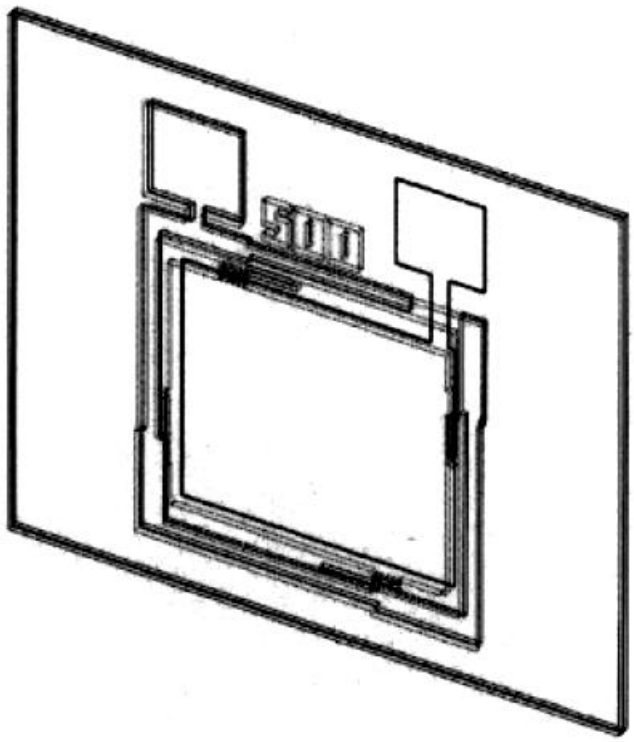

Figure 1. Capacitive microaccelerometer used for this study. Four tethers exist, one on each side of the floating plate.

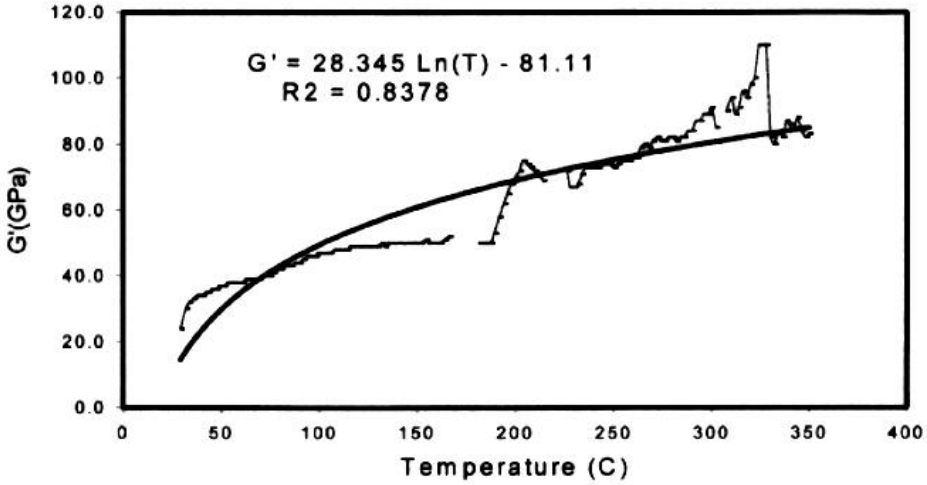

Figure 2. Typical data obtained with the Bohlin Rheometer. These results are for poly(3C-SiC). The heavy solid curve is the least squares fit to the experimental data.

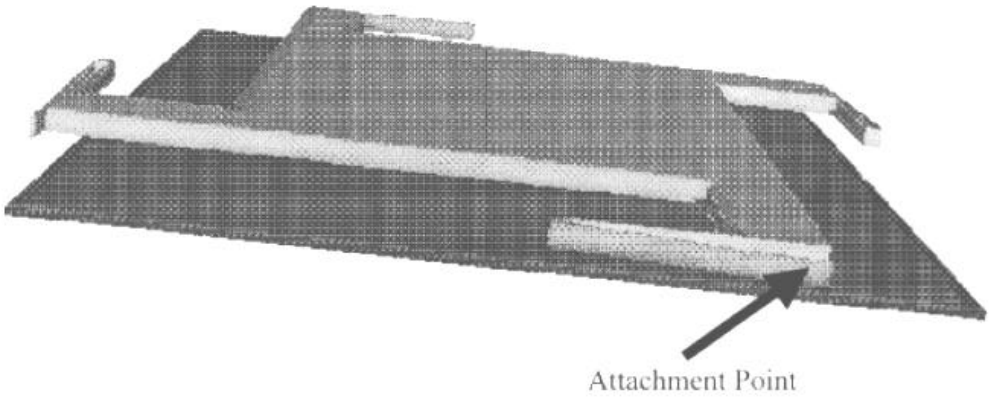

Figure 3. Solid model of device used in the simulations. The top plate thickness has been increased to show the attachment tethers. The reaction forces are at the attachments as indicated.

3 METALLIZATION OF SiC

Quantum mechanical CASTEP software calculations were performed using nickel and rhenium atom deposition onto cleaved surfaces (active, hydrogenated, and oxygenated). These calculations were performed without metal atoms and with metal atoms at selected positions (origin, a-axis, b-axis) in the unit cell. Binding energies for each of the metal atoms (nickel and rhenium) were calculated. Additionally, calculated energy bands with associated density-of-states and partial density-of-states were examined regarding the population of s, p, and d bonding characteristics. Nickel atom deposition onto silicon rich surfaces tended to bond to the silicon atoms as well as the underlying carbon atoms. However, rhenium atom deposition showed bonding only to the silicon atoms. This was observed experimentally and is reported herein. Experimentally, the rhenium deposition surface is extremely smooth and has only ohmic characteristics with near zero resistance.

3.1 Introduction

Many strides are being made in the areas of growth, doping and contamination reduction of SiC [15]. With advances in these fields, the major limiting factor in SiC device technology is reproducible metallization. Resistivities as low as 1 x 10^{-6} O/cm^2 have been achieved, however several problems remain unsolved [16]. Particularly at elevated temperatures, metal atom inter-diffusion, formation of silicates and carbides, degradation of the interface due to lattice mismatch and surface reconstruction are a few areas of research requiring more study. The most notable problem in formation of stable ohmic contacts is Schottky barrier control. Understanding what affects barrier height, how to manipulate it, and finding an appropriate metal that minimizes the barrier height while remaining harsh environment resistant will provide invaluable information for advancement in SiC device technology [17].

The encouraging experimental findings as described in the dissertation by G. Y. McDaniel [18] led us to perform the present computation. His results showed that rhenium is an excellent metal for electrical contacts to SiC. Initially he did an extensive study of the influence of thin layers of Ni on SiC to gain an understanding of contact formation. Variables affecting the work function of the SiC surface were varied and the results tabulated. Calibration during this phase of his research was unable to verify a reproducible procedure for application to the Ni/SiC contact. The Re/6H-SiC contact was demonstrated on three surfaces. Each was characterized with Dektak stylus profilometry, XRD, AES and I-V electrical measurements in the as-deposited condition. They were then exposed to a 120 minute anneal at 1000 °C in vacuum at less than 1 x 10^{-6} Torr total pressure. Each sample was again characterized and the results compared to the pre-anneal condition.

The first surface was stoichiometric clean SiC. Contacts on this surface proved to be wide ranging in resistivity depending on whether or not the contact was annealed. The pre-annealed average resistance was 3700 ohms and the average post-annealed resistance was 50 ohms. It is important to note that one sample included in this average had contact regions that were annealed at roughly 200 °C lower than other samples due to poor mounting. Removing this sample reduces the post-anneal average from 50 to only 6 ohms. The contacts were rectifying prior to

annealing. After annealing, most were still slightly rectifying, however their I-V curves indicated they were transitioning to Ohmic character. There was no detectable reaction in either XRD or AES data, however, the film was shown to relax into the (103) crystallographic plane for Re with heat treatment.

The second surface was graphitized SiC. Contacts on this surface were successful, however, their properties were undesirable for this study. In all cases, the depositions resulted in dull gray or flaky contacts and the Re did not wet with the SiC. The resistivity was less wide ranging than the stoichiometric condition. The pre-annealed average was 72 ohms and the post-annealed average was 21 ohms. All contacts were rectifying prior to annealing. After annealing again, a few contacts were near ohmic, but most still exhibited some rectifying character. There was no detectable reaction from XRD data, however, the film was shown to relax into the (002) crystallographic plane for Re with heat treatment. The AES data indicated an unusual phenomenon with this surface chemistry. While reaction was not evident, the ordering of the Re into the (002) crystallization incorporated a "self-cleaning" of the film. Films that were unintentionally contaminated with carbon throughout showed strong signs of graphite clumping and being forced to the surface of the contact with heat treatment.

The third surface was a silicon layer deposited on a stoichiometric SiC surface. This contact was the most promising of all conditions. Films were highly ordered in both the as deposited and the post-annealed conditions. XRD confirmed preferential crystallization along the Re (101) plane. AES confirmed migration of Re into the interface and possible reaction with the Si film at elevated temperatures. I-V curves prior to annealing were mostly rectifying. While annealing every contact was found to be 100% ohmic with R-squared values of 0.99 to 1.00 when subjected to a linear regression fit. The pre-anneal average resistance was 212 ohms while the post-anneal average was 3 ohms. This rhenium study was not optimized for low resistivity. Rather, it focused on material aspects; for example, the substrates used in the experimental effort did not have a heavily doped contact region.

It is this third surface condition that we chose to simulate using CASTEP software by Accelrys Inc. The modeling procedure and results of this computation follow.

3.2 Details of the Calculation

The theoretical basis of CASTEP is the density functional theory (DFT) in the local density approximation (LDA) or gradient-corrected LDA version as developed by Perdew and Wang [19] (CGA). The default setting in CASTEP is CGA. The electron-ion interaction is described using a pseudopotential concept. Potentials have been generated using the optimization scheme of Lin [20], et. al. Pseudopotentials may be either local or nonlocal, the latter in a separable Kleinman-Bylander [21] form. The action of a nonlocal potential on a wave function can be calculated in either reciprocal or real space, the real space implementation offering better scalability with size. CASTEP is based on a supercell method, whereby all studies must be performed on a specific periodic system, even when the periodicity is superficial. For example, a crystal surface must be represented by a finite-length slab. Study of molecules is also possible by assuming a molecule is put in a box and treated as a periodic system. There is no limitation on

the shape of the supercell. If the crystal possesses high point-group symmetry, this can be used to speed the calculations.

Electronic relaxation is achieved by minimization of the total energy. The electronic wavefunctions are expanded using a plane-wave basis set, and the expansion coefficients are varied so as to minimize the total energy. This minimization is implemented within CSTEP by a modern all-bands method that allows simultaneous update of all wavelengths [22]. CASTEP uses special k-points sampling for integration over the Brillouin zone, fast Fourier transforms (FFT) to evaluate matrix elements, and wavelength symmetrization for crystals with point – group symmetry higher that P1. For metallic systems CASTEP intrudes partial occupancies for levels close to the Fermi energy [23].

The procedure used was to create a 6H-SiC single crystal, minimize the structure, and cleave the crystal along a desired crystallographic plane. The distance between the cleaved surface and the bottom of the upper crystal unit cell which is in the adjacent cell, is separated to a distance sufficiently large so the surface atoms feel no interaction with the upper cell atoms, typically 50Å. Once the separation is performed, the system is again geometrically minimized. The cleave plane can be moved so as to pass through silicon atoms resulting in a silicon rich surface. This system can then be hydrogenated, oxygenated, or left stoichiometric and then again minimized. Once this minimized cleaved surface structure is achieved, all atom positions below the top layer were fixed. Any minimizations hereafter will only move the surface and deposited atoms.

The standard pseudopotentials used were in Kleinman-Bylander [21] separable form and are norm conserving. This guarantees the transferability of the pseudopotential. That is, the same potential correctly reproduces the valence electron scattering by the ionic core in different chemical environments. Potential for the first-row elements (C, O, N, etc.) and for transition metals are optimized to achieve the best possible convergence with respect to the number of plane waves in the basis set. For rhenium we used the CASTEP in pseudopotential, cst_Re_00.usp. We used the GGS-RPBE pseudopotentials as provided in CASTEP. This is the spin-polarized version of the Generalized Gradient approximation using the revised Perdew-Burke-Ernzerhof potentials [24-27].

The k-point selection in CASTEP uses the Monkhorst-Pack scheme [28], which produces a uniform mesh in reciprocal space. For all calculations, we specified the energy convergence criterion to be 0.1 eV/atom.

Once the unit cell atom configuration was minimized, a rhenium atom was added at selected positions (typically at the origin, the end of the a-axis and the end of the b-axis). It was placed at roughly 2.0Å above the surface of the silicon atoms. A single-point energy minimization was performed. The global energy minimum was chosen as the best attachment position. Using the Cerius2 software, bonds to the neighboring atoms were formed. Then a 2 x 2 superlattice was formed by combining four basic unit cells and a single rhenium atom was added at specific locations and the system minimized. After this a 3 x 3 superlattice was formed using nine unit cells and at selected points on the surface a rhenium atom was inserted for minimization. This

procedure allows the investigator to extrapolate the binding energy of rhenium to that of an infinite silicon rich surface.

3.3 Computational Results

As mentioned above, the metallization of a silicon rich 6H-SiC surface with nickel led to a surface with poor current carrying characteristics and which clustered when annealed at elevated temperatures, about 1000 °C. Computationally, nickel atoms deposited onto a silicon rich cleaved (001) 6H-SiC surface bonded to the silicon atoms and to the underlying layer of carbon atoms, Figure 4. The partial density-of-states is shown in Figure 5. In this plot the Fermi level is located at zero eV. One can see that nickel deposited onto silicon acts as a semiconductor. The top of the valence band is dominated by d-type wave functions. There is some p-type character. The bottom of the conduction band is dominated by d-type bonding but also has an almost equally strong p-type and s-type bonding character. For nickel with three bonds to silicon and one to carbon, the average bond energy is 427 kJ/mole (102 kcal/mole). The binding energy of nickel to the cleaved silicon rich surface is 1,868 kJ/mole (446.26 kcal/mole).

Experimentally, rhenium atoms deposited onto a silicon rich 6H-SiC surface and annealed for 120 minutes at 1000 °C yielded a smooth, very low resistance, purely ohmic electrical contact. As above for nickel atoms, rhenium was placed over selected positions in the unit cell, e.g., over the origin (O), at the end of the b-axis (B), and at the end of the a-axis (A), see Figure 6. Here we report the results of placing the atom over the origin. The total energy of the system varied only by about one percent between using an active surface, a silicon rich, or a hydrogenated silicon surface. Since the experiments dealt with silicon rich surfaces and small variations existed between various surface conditions, we will report only on silicon rich surface conditions. Rhenium bonded only to the silicon atoms. Even when we created a carbon rich surface, the rhenium atoms bonded to the underlying silicon atoms. For the silicon rich surface, the average bond energy was 846 kJ/mole (202 kcal/mole). The binding energy of rhenium to the silicon rich surface was 991 KJ/mole (236.6 kcal/mole). The width of the unit cell surface was increased from a 1 x 1 cell to a 2 x 2 to a 3 x 3 cell size. The average bond energy remained about the same. The partial density-of-states for rhenium atoms deposited onto a silicon rich 6H-SiC surface is presented in Figure 7. Here the Fermi energy is located at 0 eV. The s-type wave function extends above the Fermi level. There appears to be no d-type bonding. When we deposited a second layer of rhenium atoms onto the first layer, Figure 8, we now observed a total metal material (Figure 9). The s-, p-, and d-type wave functions all extend through the Fermi level into the conduction band. There is no bandgap; the material is a metal.

3.4 Conclusions

Calculations show that the bond energy of rhenium to a silicon rich surface is about twice that of nickel to the same surface. This helps explain the better stability of rhenium over nickel on a silicon rich surface of 6H-SiC after annealing at 1000 °C for 120 minutes. This selected bonding of rhenium atoms to only silicon atoms was independently determined computationally. It was only after we presented the computational results that we heard about the experimental findings.

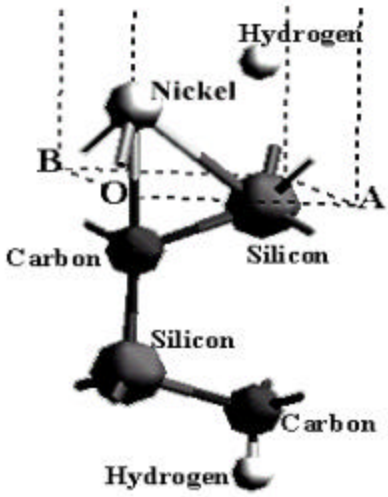

Figure 4. Single cell showing first layer deposition nickel atoms bonding to silicon and underlying carbon atoms.

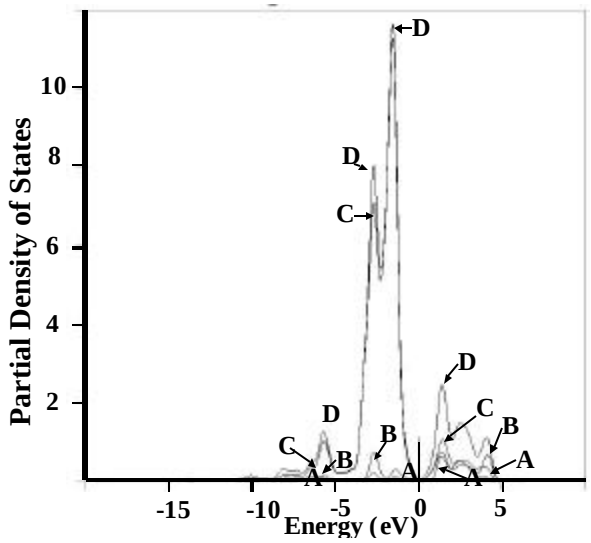

Figure 5. Partial density-of-states of first layer bonding of nickel to silicon and underlying carbon atoms. Curves are designated, A, total s-type bonding; B, total p-type bonding, and D, total sum bonding.

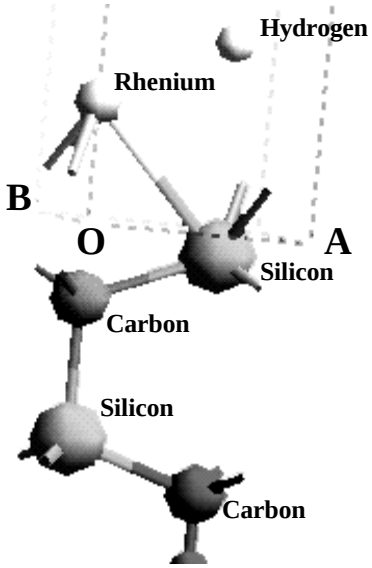

Figure 6. Single cell showing first layer deposition rhenium atoms bonding only to silicon atoms.

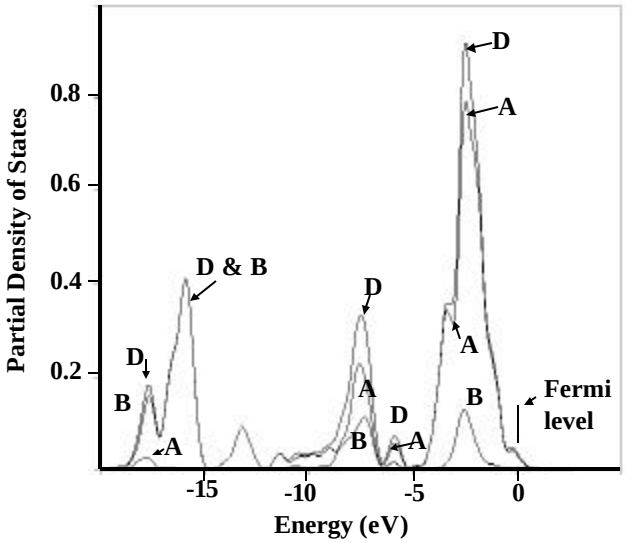

Figure 7. Partial density-of-states of first layer bonding of rhenium to silicon atoms. Curves are designated, A, total s-type bonding; B, total p-type bonding, and D, total sum bonding.

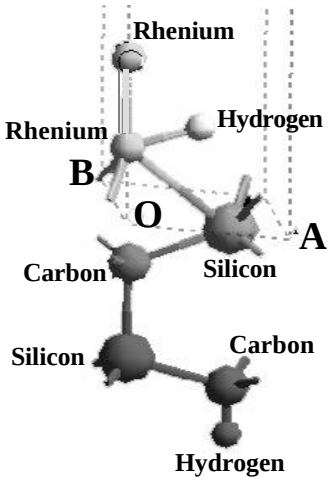

Figure 8. Single cell showing second layer deposition rhenium atoms onto the first layer of rhenium atoms, which bonded only to silicon atoms. The second layer bonds only to the existing layer of rhenium atoms.

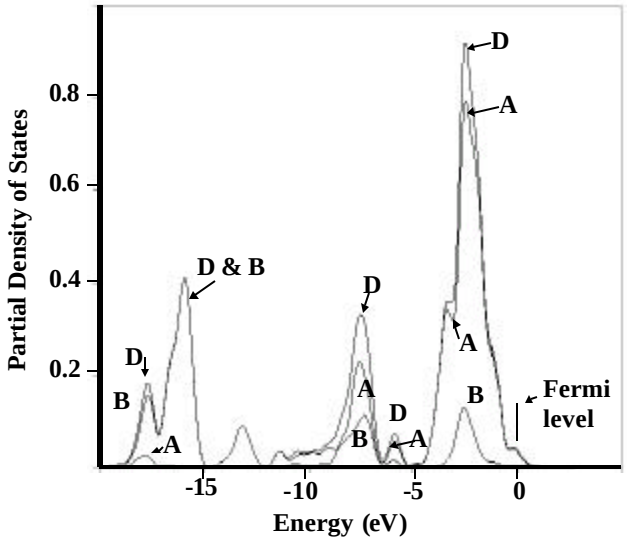

Figure 9. Partial density-of-states of second layer bonding of rhenium on rhenium, which is on a silicon rich surface. Curves are designated, A, total s-type bonding; B, total p-type bonding, C, d-type bonding and D, total sum bonding.

4 CONCLUSIONS

The results from this program provide clear evidence of the benefit of SiC as a harsh environment (specifically high temperature) material for both structural and electronic devices. Although shock testing of SiC MEMS devices under this program was not accomplished, subsequent work allowed for this testing to occur, with positive results. Furthermore, one of the key concerns with respect to SiC electronics was the need for good contact metallization for ohmic contacts. Rhenium was found to be an excellent material for providing ohmic contact metallization on SiC. These results provide a good foundation for the benefits of SiC for harsh environment (high temperature and high shock) applications.

5 REFERENCES

1. Atwell, Andrew R., Okojie, Robert S., Kornegay, Kevin T., Roberson, Scott L., and Beliveau, Alain, "Simulation, fabrication and testing of bulk micromachined 6H-SiC high-*g* piezoresistive accelerometers," *Sensors and Actuators A*, **104**, 11-18 (2003).
2. S. Morkoc, S. Strite, G. B. Gao, M.E. Lin, B. Sverdlov, and M. Burns, *J. Appl. Phys*., **76**, 1363-1371 (1994).
3. Robert A. Metzger, *Compound Semiconductors*, **1**, 26-28 (1995).
4. Thadeus B. Massalski, Binary Alloy Phase Diagrams, 590 (1986).
5. Papanicolaou, A. Hristou, and M. L. Gipe, *J. Appl. Phys*., **65**, 3526-3530 (1989).
6. Moki, A. P. Shenoy, D. Alok, and B. J. Baliga, *J. Elect. Mat*., **24**, 315-317 (1995).
7. J. B. Hudson, Surface Science, An Introduction, Butterworth-Heinemann, Boston, 236-244 (1992).
8. Rolf E. Hummel, Electronic Properties of Materials, Springer-Verlag, Berlin, 98-119 (1993).
9. G. L. Katulka, J. Kolodzey, and J. Olowolafe, *IEEE Trans. Mag*., **35**, 356-360 (1999).
10. M. Manudurand and Sijiro Furukawa, *IEEE J. Circ. & Dev*., **8**, 22-26 (1992).
11. S. P. Timenshenko and J. N. Goodier, Theory of Elasticity, 3rd Ed., McGraw-Hill, 309-313 (1970).
12. S. P. Timenshenko, Strength of Materials Part II, 3rd Ed., Van Nostrand, 286-291 (1956).
13. M. Mehregany, CWRU, SiC MUSiC Process
14. M. Paz, Structural Dynamics Theory and Computations, Van Nostrand Reinhold (1991).
15. Photoemission work currently being studied at Wright-Patterson AFB, Ohio.
16. Tsutomu Uemoto, *Jap. J. Appl. Phys*., **34**, L7-L9 (1995).
17. M. J. Bozack, *Phy. Stat. Sol. (b)*, **202**, 549-580 (1997).
18. G. Y. McDaniel, PhD Dissertation, Dept. Physics, University of Florida (2001).
19. J. P. Perdew, Electronic Structure of Solids, ed; P. Ziesche and H. Eschrig, Berlin Akademie, (1991).
20. Z. Lin and J. Harris, *J. Phys. Condens. Matter*, **5**, 1055 (1992).
21. L. Kleinman and D. M. Bylander, *Phys. Rev. Lett*., **44**, 1425 (1982).
22. J. Gillan, *J. Phys. Cond. Matt*., **1**, 689 (1989).
23. A. de Vita, Ph. D. Thesis, Keele Univ., UK (1992).
24. J.P. Perdew and Y. Wang, *Phys. Rev*., **B46**, 6671 (1992).
25. J.A. White and D.M. Bird, *Phys. Rev*., **B50**, 4954 (1994).
26. J.P. Perdew, K. Burke, and M. Ernzerhof, *Phys. Rev. Lett*., **77**, 3865 (1996).
27. B. Hammer, L.B. Hansen, and J.K. Norskov, *Phys. Rev*., **B59**, 7413 (1999).
28. H. J. Monkhorst and J. D. Pack, *Phys. Rev*., **B13**, 5188 (1976).

DISTRIBUTION LIST
AFRL-MN-EG-TR-2004-7025

Defense Technical Info. Center 8725 John J. Kingman Rd Ste 0944 Fort Belvoir VA 22060-6218	1

Eglin AFB offices:

AFRL/MNOC-1 (STINFO Office)	1
AFRL/CA-N	1
AFRL/MNME	1
AFRL/MNMF	1
AFRL/MNMW	1
AFRL/MNMI	1
AFRL/MN	1